Journal of Medicinal Chemistry

Article

pubs.acs.org/jmc

Exploring the Influence of the Protein Environment on Metal-Binding Pharmacophores

David P. Martin,[†] Patrick G. Blachly,[†] J. Andrew McCammon,[†,‡,§] and Seth M. Cohen*[,†]

[†]Departments of Chemistry and Biochemistry, [‡]Pharmacology, and [§]Howard Hughes Medical Institute, University of California, San Diego, 9500 Gilman Drive, MC 0358, La Jolla, California 92093, United States

Supporting Information

ABSTRACT: The binding of a series of metal-binding pharmacophores (MBPs) related to the ligand 1-hydroxypyridine-2-(1*H*)-thione (1,2-HOPTO) in the active site of human carbonic anhydrase II (hCAII) has been investigated. The presence and/or position of a single methyl substituent drastically alters inhibitor potency and can result in coordination modes not observed in small-molecule model complexes. It is shown that this unexpected binding mode is the result of a steric clash between the methyl group and a highly ordered water network in the active site that is further stabilized by the formation of a hydrogen bond and favorable hydrophobic contacts. The affinity of MBPs is dependent on a large number of factors including donor atom identity, orientation, electrostatics, and van der Waals interactions. These results suggest that metal coordination by metalloenzyme inhibitors is a malleable interaction and that it is thus more appropriate to consider the metal-binding motif of these inhibitors as a pharmacophore rather than a "chelator". The rational design of inhibitors targeting metalloenzymes will benefit greatly from a deeper understanding of the interplay between the variety of forces governing the binding of MBPs to active site metal ions.

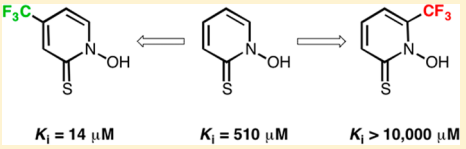

INTRODUCTION

Metalloenzymes, those which require a metal ion cofactor to function, are an emerging class of therapeutic targets.[1,2] Inhibitors targeting carbonic anhydrases (CAs, Zn^{2+}-dependent),[3] angiotensin converting enzyme (ACE, Zn^{2+}-dependent),[4] histone deacetylases (HDACs, Zn^{2+}-dependent),[5] 5-lipoxygenase (5-LO, $Fe^{2+/3+}$-dependent),[6] and HIV integrase (HIV1-IN, Mg^{2+}-dependent)[7] are clinically approved for the treatment of glaucoma, hypertension, cutaneous T-cell lymphoma, asthma, and HIV infection, respectively. Furthermore, inhibitors targeting these and other metalloenzymes are in various stages of clinical trials for the treatment of a wide variety of ailments including bacterial and viral infection, hypertension, cancer, and inflammation. For the most part, metalloenzyme inhibitors contain pharmacophores that bind directly to the catalytic metal ion of the target.[8] Given the extensive structural optimization that goes into clinical candidates, it is surprising how little diversity there is in the metal-binding pharmacophores (MBPs) utilized in metalloenzyme inhibitor design; thiols, carboxylic acids, phosphates, and hydroxamic acids have historically dominated the chemical landscape for binding active site metal ions. However, this has begun to change as illustrated by the emergence of inhibitors targeting HIV1-IN that utilize innovative hetrocyclic MBPs as well as HDAC inhibitors containing the unconventional *N*-(2-aminophenyl)benzamide MBP.[9] The latter example is especially interesting because it is a scaffold that would not be considered a strong metal-binding motif but nonetheless strongly inhibits certain HDAC isoforms by maximizing other interactions with the active site. In addition, for nearly a decade, our laboratory has proposed alternative metal-binding scaffolds, which have been evaluated against a wide range of metalloprotein targets.[10−16]

The utilization of novel MBPs has the potential to improve both the target specificity and pharmacokinetic properties of metalloenzyme inhibitors, thereby improving the clinical success rate of this class of therapeutics. Numerous studies have demonstrated that MBP optimization can aid in designing selective and/or potent inhibitors for a variety of metalloenzyme targets.[17−22] The use of structure-aided design can be invaluable to this process, but due to the complexity of the metal−inhibitor interaction, computational protocols to accurately predict the binding mode and potency of MBPs have been elusive.[23−25] Consequently, in the absence of explicit structural data, assumptions (e.g., bond lengths and coordination geometry) must be made about the MBP−metalloenzyme interaction. In some cases, these parameters have been estimated based on the structure of MBPs bound to small-molecule model complexes, but these models do not account for the constrained environment and nuanced features found in a metalloenzyme active site.[11,26−30] Consistent with the aforementioned limitations, previous studies have shown that the coordination modes of α-mercaptoketone (mono- vs bidentate coordination), *N*-hydroxyurea (*N*-hydroxyl vs carbonyl monodentate coordination), and 3-hydroxy-(1*H*)-pyridin-2-one (orientation of bidentate coordination) MBPs can be changed based on relatively subtle changes in the structure of the inhibitor backbone,[31−33] an effect that would not be recapitulated in model compounds.

Received: July 1, 2014
Published: August 12, 2014

   dx.doi.org/10.1021/jm500984b | *J. Med. Chem.* 2014, 57, 7126−7135

Because of many characteristics including its rigid structure, stability, and ease of crystallization, human carbonic anhydrase II (hCAII) is an excellent protein model system for examining MBP−metalloenzyme interactions.[34] The active site consists of a His_3-bound Zn^{2+} ion that sits in a relatively solvent-exposed depression (Figure 1). Arylsulfonamide MBPs are used in CA

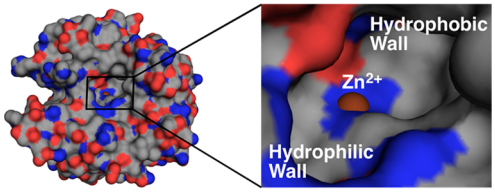

Figure 1. Structure of hCAII (PDB 3KS3). The active site Zn^{2+} ion (shown in bronze) sits at the bottom of a cone-shaped depression containing both hydrophobic and hydrophilic walls.

inhibitors and are prime examples of the effect that the active site environment can have on enhancing MBP binding. Although the sulfonamide MBP shows little activity against other metalloprotein targets, it has very high activity against CAs, which has been attributed to the MBP being optimally positioned for hydrogen bonding with active site residues upon metal binding (Figure 2A). Recently, we reported that in the

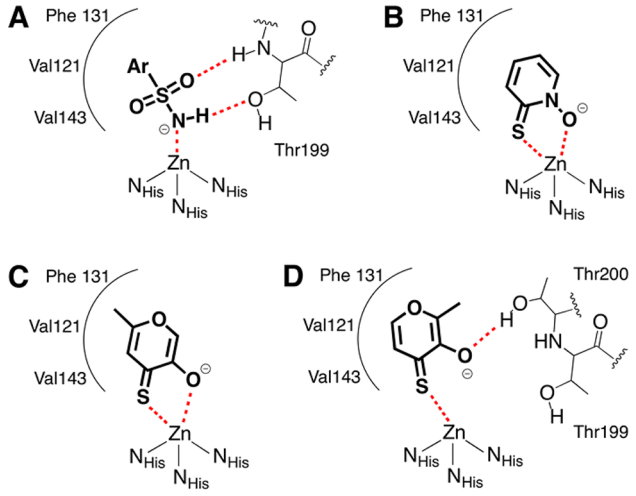

Figure 2. Diagram of MBP binding modes in the active site of hCAII. (A) Aryl sulfonamides are positioned for hydrogen bonding upon metal coordination. (B) 1-Hydroxypridine-2-(1*H*)-thione (1,2-HOPTO, PDB 3M1K) acts as a bidentate ligand. (C) The MBP allothiomaltol (PDB 4MLX) also shows bidentate coordination, but its isomer thiomaltol (D, PDB 4MLT), which differs only in the position of a methyl group, adopts monodentate coordination.

active site of hCAII, 3-hydroxy-(4*H*)-pyran-4-thione derivatives differing only in the presence or position of a single methyl group show different binding modes (Figure 2B−D), including unexpected monodentate coordination to the Zn^{2+} ion by thiomaltol (TM, Figure 2D).[35]

To understand the origin of the unique coordination mode adopted by TM in the active site of hCAII and, more generally, gain greater insight into the influence of active site environments on MBP−metalloprotein interactions, this study examines the binding of a series of related MBPs based on 1-hydroxypyridine-2-(1*H*)-thione (1,2-HOPTO, Figure 2) to hCAII. This MBP was chosen because it has been previously reported to be a moderate inhibitor of hCAII, binding in a bidentate fashion to the active site Zn^{2+} ion (Supporting Information, Figure S2), and derivatives with substituents on the ring of the ligand can be readily synthesized.[36] We find that a methyl group appended to the 1,2-HOPTO scaffold in a position analogous to that of TM results in the MBP (6-CH_3-1,2-HOPTO) adopting a similar monodentate coordination mode. Furthermore, we show that the unexpected coordination modes of these MBPs are likely the result of a significant energetic penalty for disrupting the highly ordered water network within the active site and are stabilized by favorable interactions with the hydrophobic wall of the active site. The relationship between metal coordination and other MBP−metalloenzyme interactions is examined, showing that no single interaction is dominant, but rather that the binding of these molecules is influenced by a combination of a number of interdependent forces. The results show that canonical metal "chelators" used in metalloenzyme inhibitors are better described as malleable pharmacophores, hence our suggestion of the term "metal-binding pharmacophore".

RESULTS

Methyl 1,2-HOPTO Derivatives. Previous studies have shown that a single methyl substituent on the 3-hydroxy-(4*H*)-pyran-4-thione MBP can alter its coordination mode in the active site of hCAII.[35] It was hypothesized that because the steric restrictions of the active site force MBPs into nonideal coordination, other ligand−protein interactions could influence the coordination mode. To further understand these effects, a series of methyl derivatives of the 1,2-HOPTO scaffold were synthesized (Figure 3) and their inhibitory activity against hCAII was investigated (Table 1). The previously reported crystal structure of 1,2-HOPTO bound to hCAII shows that the MBP coordinates the active site Zn^{2+} ion in a bidentate fashion, resulting in a distorted trigonal bipyramidal geometry.[36] The sulfur atom of 1,2-HOPTO acts as an equatorial donor while the oxygen atom acts as an axial donor, orienting the sulfur toward the hydrophobic wall of the active site (see Supporting Information, Figure S2). Derivatives of 1,2-HOPTO with a methyl group positioned toward the hydrophobic wall (3-CH_3-1,2-HOPTO and 4-CH_3-1,2-HOPTO) show over a 10-fold increase in potency over unsubstituted 1,2-HOPTO (Table 1). When the substituent is in a position that, based on the 1,2-HOPTO crystal structure, would not be oriented toward either active site wall (e.g., 5-CH_3-1,2-HOPTO), inhibition is only slightly improved. Importantly, when a methyl group is positioned toward the hydrophilic side of the active site (6-CH_3-1,2-HOPTO), significantly weaker inhibition is observed (Table 2) when compared to 1,2-HOPTO.

To understand the inhibition data reported in Table 2, the crystal structures of 3-CH_3-, 4-CH_3-, and 5-CH_3-1,2-HOPTO bound in the active site of hCAII were determined. All of these derivatives show bidentate coordination by the MBPs (Figure 4), identical to that of unsubstituted 1,2-HOPTO. The methyl group of 3-CH_3-1,2-HOPTO makes hydrophobic contacts with the side chains of Val143, Leu198, and Val12 (see Supporting Information, Figure S4), while the methyl group of 4-CH_3-1,2-HOPTO is positioned slightly further out of the active site, interacting with Val121, Leu198, and Phe131 (see Supporting Information, Figure S5). As predicted, the methyl group of 5-CH_3-1,2-HOPTO does not make any significant contacts (<4.5 Å) with the hydrophobic wall; the only active site residue in

dx.doi.org/10.1021/jm500984b | J. Med. Chem. 2014, 57, 7126−7135

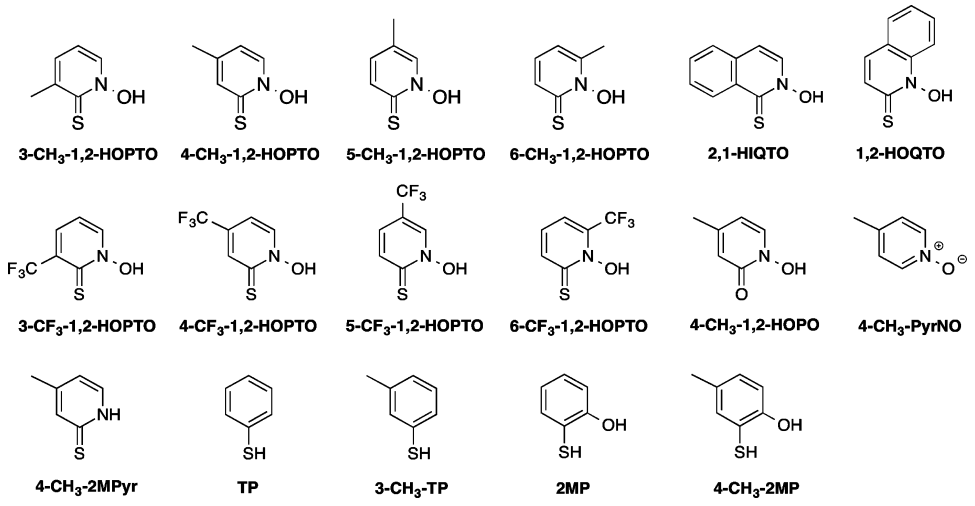

Figure 3. Structures and naming of MBPs.

Table 1. K_i Values (μM) of Methyl Derivatives of 1,2-HOPTO against hCAII

compd	K_i	compd	K_i
1,2-HOPTO	510 ± 90	5-CH_3-1,2-HOPTO	260 ± 20
3-CH_3-1,2-HOPTO	48 ± 5	6-CH_3-1,2-HOPTO	2300 ± 200
4-CH_3-1,2-HOPTO	38 ± 5	4,6-CH_3-1,2-HOPTO	950 ± 100

Table 2. K_i Values (μM) of 1,2-HOPTO Derivatives with Larger Substituents against hCAII

compd	K_i	compd	K_i
3-CF_3-1,2-HOPTO	64 ± 5	6-CF_3-1,2-HOPTO	>10000
4-CF_3-1,2-HOPTO	14 ± 3	2,1-HIQTO	2300 ± 200
5-CF_3-1,2-HOPTO	270 ± 30	1,2-HOQTO	950 ± 100

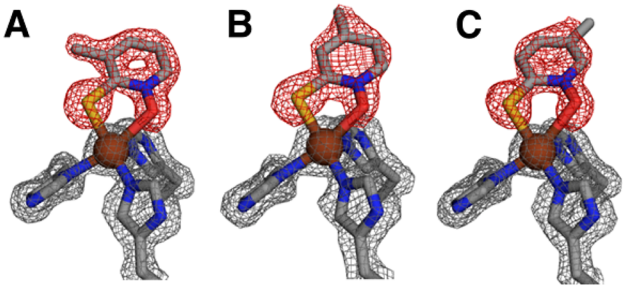

Figure 4. Crystal structures of 3-CH_3-1,2-HOPTO (A), 4-CH_3-1,2-HOPTO (B), and 5-CH_3-1,2-HOPTO (C) bound to hCAII. All show bidentate coordination similar to unsubstituted 1,2-HOPTO (Supporting Information, Figure S2). The $|2F_o - F_c|$ map (1.5σ) is shown in gray for the Zn^{2+} ion and protein residues while the omit $|F_o - F_c|$ map (4.0σ) is shown in red for the ligands. For clarity, only the metal active site is shown.

close proximity to the methyl group is the side chain amide of Gln92 (3.7 Å, see Supporting Information, Figure S6).

The crystal structure of 6-CH_3-1,2-HOPTO bound in the active site of hCAII reveals that its decreased inhibitory activity is accompanied by a shift to monodentate coordination in the active site of hCAII (Figure 5A). The Zn−S distance (2.3 Å) is consistent with those in previously reported structures of monodentate sulfur donors bound to active site Zn^{2+} ions.[37] The hydroxyl group, which is 3.5 Å from the metal ion, remains oriented toward the hydrophilic side of the active site, forming a close interaction with the side chain of Thr200 (2.9 Å,

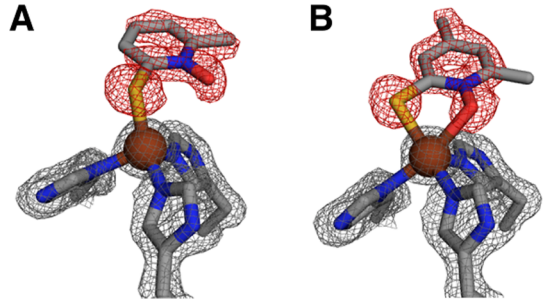

Figure 5. Crystal structure of 6-CH_3-1,2-HOPTO (A) bound to hCAII shows monodentate coordination while that for 4,6-CH_3-1,2-HOPTO (B) shows that bidentate coordination is stabilized by the presence of a methyl group in the 4-position. The $|2F_o - F_c|$ map (1.5σ) is shown in gray for the Zn^{2+} ion and protein residues while the omit $|F_o - F_c|$ map (3.5σ) is shown in red for the ligands. For clarity, only the metal active site is shown.

Supporting Information, Figure S7). The change in coordination also places 6-CH_3-1,2-HOPTO closer to the hydrophobic wall so that the ring of the ligand makes contacts with Val121 and Val143 in addition to an improved interaction with Leu198 (~0.2 Å closer) relative to unsubstituted 1,2-HOPTO (see Supporting Information, Figure S7). Because a methyl group in the 6-position appears to destabilize bidentate coordination, 4,6-CH_3-1,2-HOPTO, which has methyl groups in the 4- and 6-position, was synthesized. While this MBP shows more than a 20-fold decrease in affinity relative to 4-CH_3-1,2-HOPTO, the crystal structure of 4,6-CH_3-1,2-HOPTO bound to hCAII shows that bidentate coordination is maintained with the 6-methyl group extending toward the hydrophilic region of the active site (Figure 5).

Larger Hydrophobic Substituents. The relatively solvent-exposed methyl group of 5-CH_3-1,2-HOPTO and the monodentate coordination of 6-CH_3-1,2-HOPTO when bound to hCAII suggest that there is a significant penalty for swapping

dx.doi.org/10.1021/jm500984b | J. Med. Chem. 2014, 57, 7126−7135

the position of the coordinating atoms of 1,2-HOPTO. That is, rotation of the MBP by 180° so that the oxygen atom is on the hydrophobic side of the active site and the sulfur atom is on the hydrophilic side would position the methyl groups of these two ligands to make favorable hydrophobic interactions similar to those made by 3-CH_3-1,2-HOPTO and 4-CH_3-1,2-HOPTO. However, this change in donor atom position is not observed. We reasoned that if functional groups could be added to the 1,2-HOPTO scaffold that improve these hydrophobic interactions, this barrier might be overcome for ligands with substitutions in the 5- or 6-position. With this goal in mind, 1,2-HOPTO ligands were synthesized with trifluoromethyl and aryl groups appended (Figure 3). A slight decrease in potency is observed for 3-CF_3-1,2-HOPTO relative to its methyl analogue (64 vs 48 μM), while the same substitution in the 4-position leads to an improvement in potency (14 μM for 4-CF_3-1,2-HOPTO vs 38 μM for 4-CH_3-1,2-HOPTO). The inhibitory activity of 5-CF_3-1,2-HOPTO is essentially unchanged from the methyl analogue, while all activity is lost with a trifluoromethyl group in the 6-position (6-CF_3-1,2-HOPTO). Addition of a second, fused aromatic ring to the 3/4-positions of the 1,2-HOPTO scaffold also results in a significant increase in binding affinity (2-hydroxyisoquinoline-1-(2*H*)-thione, 2,1-HIQTO, K_i = 15 μM) but results in slightly diminished activity when appended to the 5/6-positions (1-hydroxyquinoline-2-(1*H*)-thione, 1,2-HOQTO, K_i = 730 μM).

The binding modes of 3-CF_3-1,2-HOPTO and 4-CF_3-1,2-HOPTO to hCAII were determined and were found to be similar to their corresponding methyl analogues (Supporting Information Figures S8 and S9). The trifluoromethyl groups are highly ordered in both structures, suggesting that their interactions with the hydrophobic wall of the active site are quite favorable. The crystal structure of 5-CF_3-1,2-HOPTO bound to hCAII shows two different binding modes, each with ~50% occupancy (see Supporting Information, Figure S10). In the first, the ligand is in fact "flipped" 180° and coordinated in a bidentate fashion with the sulfur atom on the hydrophilic side of the active site and the oxygen atom closer to the hydrophobic wall. This switch in donor arrangement relative to the other 1,2-HOPTO derivatives places the trifluoromethyl group of 5-CF_3-1,2-HOPTO in the same position as that of 4-CF_3-1,2-HOPTO (Figure 6). The S–Zn distance (2.2 Å) is much shorter than the O–Zn distance (2.6 Å), and the coordination geometry remains trigonal bipyramidal with the oxygen atom as an axial donor. In the second binding mode, there appears to be no metal coordination, as both the S–Zn distance (3.4 Å) and O–Zn distance (4.3 Å) are too long for the donors to have any significant interaction with the Zn^{2+} ion. Instead of metal coordination, the oxygen atom sits in a hydrophilic pocket lined by hydrogen bond donors including the backbone amide nitrogen of Thr199 (3.0 Å) and the backbone amide nitrogen (3.2 Å) and side chain (3.4 Å) of Thr200 (see Supporting Information, Figure S10). The position of this oxygen atom does not correspond to that of a water molecule in the inhibitor-free structure of hCAII. In this orientation, the ring of 5-CF_3-1,2-HOPTO is positioned to make contacts with Val121 (3.4–4.0 Å) and Leu198 (3.9 Å), while the trifluoromethyl group interacts with Phe131 (3.4–4.0 Å).

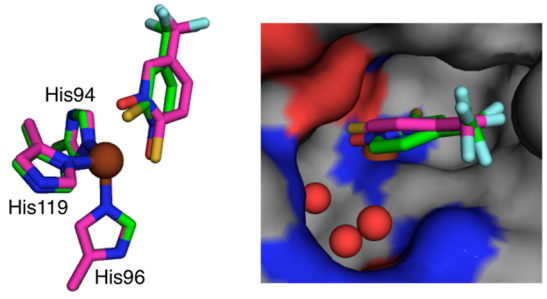

Figure 6. Two views of the crystal structure of 5-CF_3-1,2-HOPTO (carbon atoms in magenta) bound to hCAII show "flipped" coordination relative to 4-CF_3-1,2-HOPTO (carbon atoms in green), positioning the CF_3 groups similarly in the active site. Analysis of the Zn^{2+} coordination shows nearly ideal trigonal bipyramidal geometry. Conserved water molecules in the hCAII active site are shown as red spheres.

The crystal structure of 2,1-HIQTO bound to hCAII shows coordination similar to 1,2-HOPTO (see Supporting Information, Figure S11). Consistent with the significant increase in potency relative to the unsubstituted 1,2-HOPTO MBP, this binding mode positions the fused aromatic ring for extensive interactions with the hydrophobic wall of the active site including Val 143 (3.9 Å), Val121 (3.5–4.0 Å), Leu198 (3.7–4.0 Å), and Phe131 (4.0 Å). Attempts at soaking 1,2-HOQTO into the active site of hCAII led to diffuse electron density that suggested two binding modes similar to those of 5-CF_3-1,2-HOPTO; the complex could not be adequately modeled, likely due to a combination of the low affinity and solubility of the ligand as well as disordered binding (data not shown).

4-CH_3-1,2-HOPTO Derivatives with Altered Donor Sets. The divergent affinities and binding modes observed for 6-CH_3-1,2-HOPTO and 5-CF_3-1,2-HOPTO indicate that the coordinative ability of the MBP does not completely dominate the strength and geometry of binding. To examine this, MBP derivatives of 4-CH_3-1,2-HOPTO with alternative donor sets were synthesized (Figure 3). 2-Mercapto-4-methylpyridine (4-CH_3-2MPyr) contains the same sulfur donor as 4-CH_3-1,2-HOPTO but lacks the oxygen donor and, as a result, is ~200-fold less active against hCAII (K_i = 7.0 mM). The corresponding pyridine-*N*-oxide (4-CH_3-PyrNO) with the sulfur donor removed shows no measurable inhibition of hCAII. The 1-hydroxypyridin-2-(1*H*)-one analogue (4-CH_3-1,2-HOPO), which has an oxygen donor instead of sulfur, is more than 30-fold less potent than 4-CH_3-1,2-HOPTO. These results suggest that although the MBP interactions are malleable, maintaining strong coordination to the metal ion is important for good inhibitory activity.

Much like its thione analogue, 4-CH_3-1,2-HOPO acts as a bidentate ligand to the Zn^{2+} ion of hCAII (see Supporting Information, Figure S12A), with the nitrogen-bound oxygen as the axial donor (2.1 Å) and the carbonyl oxygen as the equatorial donor (2.2 Å). This is the reverse of the binding mode predicted by the $Tp^{Ph,Me}$ model complex in which the carbonyl oxygen is the axial donor. The MBP is positioned such that the methyl group forms contacts with the hydrophobic wall of the active site similar to those made by 4-CH_3-1,2-HOPTO. A water molecule sits above the donor atoms, interacting with the Zn^{2+}-bound carbonyl oxygen of 4-CH_3-1,2-HOPO (2.8 Å) as well as both the backbone amide NH (2.9 Å) and side chain (2.8 Å) of Thr199. This water molecule is not present in any of the bidentate 1,2-HOPTO structures. The side chain of Thr200 is also rotated such that there is no interaction between it and the *N*-hydroxyl group of 4-CH_3-1,2-HOPO (4.5 Å).

dx.doi.org/10.1021/jm500984b | J. Med. Chem. 2014, 57, 7126–7135

The crystal structure of 4-CH_3-2MPyr bound to hCAII shows that, despite the lack of an oxygen donor, the ligand is oriented in the active site in a very similar position to that of 4-CH_3-1,2-HOPTO, with the sulfur atom bound to the Zn^{2+} ion (2.3 Å) and the methyl group interacting with the hydrophobic wall (see Supporting Information, Figure S12B). The endocyclic nitrogen atom does not interact with active site protein residues but is in the proximity of a water molecule (2.8 Å) that in turn interacts with the side chains of both Thr199 (2.8 Å) and Thr200 (2.7 Å). This water molecule does not appear in either inhibitor-free hCAII (PDB 3KS3) or in the structures of other monodentate inhibitors bound in the active site.

Although they are structurally similar to 4-CH_3-2MPyr, aromatic thiols such as thiophenol and 2-mercaptophenol (TP and 2MP, Figure 3) have been previously reported to inhibit hCAII with K_i values in the low micromolar range.[38] To determine whether the interactions perturbing 1,2-HOPTO binding apply to other MBPs containing similar donor sets, methyl derivatives of TP and 2MP analogous to 4-CH_3-1,2-HOPTO were obtained and their binding to hCAII investigated. While 3-CH_3-TP has similar inhibitory activity to unsubstituted TP (K_i = 2.1 μM vs 3.5 μM), the 4-methyl analogue of 2MP is significantly more potent (0.52 vs 3.1 μM). Remarkably, the activity of 4-CH_3-2MP is the same as benzenesulfonamide (BSA, K_i = 0.49 μM),[39] the parent MBP of all FDA-approved CA inhibitors, illustrating the benefit that a rational approach to MBP design that includes both metal coordination and MBP−protein interactions can have.

The crystal structure of 3-CH_3-TP to hCAII reveals monodentate coordination to the Zn^{2+} ion similar to that previously reported for 2MP (see Supporting Information, Figure S13), and the binding mode is very similar to that of 6-CH_3-1,2-HOPTO. The methyl group does not interact with the hydrophobic wall of the active site and is relatively solvent exposed aside from a close contact (3.8 Å) with the side chain of Gln92. However, the aromatic ring of the ligand makes extensive contacts with Val121 (3.6−3.9 Å), Val143 (3.8 Å), and Leu198 (3.8−4.0 Å). The binding of 4-CH_3-2MP is essentially the same, but the hydroxyl group extends toward the hydrophobic wall, making additional contacts with Val143 and Trp209 (see Supporting Information, Figure S14).

Energetic Contributions to MBP Binding Affinities. To assess the electronic effects of methyl and trifluoromethyl substituents at the 4-position of 1,2-HOPTO, energy decomposition analyses (EDAs) were performed and compared with experimental binding affinities (Table 3). All EDA computations are performed on two different geometries of the Tp^CZn(MBP) complex: (a) a freely optimized Tp^CZn-(MBP) complex, where the binding orientation of the MBP is ideal (denoted "ideal" in Table 3), and (b) a constrained Tp^CZn(MBP) complex, where the angle between the plane of the MBP and the plane comprising the pyrazole nitrogens that coordinate Zn^{2+} (ϕ) is set to ∼130° (see Supporting Information, Figure S3), roughly mimicking the conformation from the crystal structure of 1,2-HOPTO bound to hCAII (denoted "protein" in Table 3).

Considering first the freely optimized Tp^CZn(MBP) complexes (optimized geometries shown in the Supporting Information, Figure S15), the 4-CH_3-1,2-HOPTO MBP is observed to interact more favorably with Tp^CZn (ΔE_{Tot} = −266.9) than either 1,2-HOPTO (−263.7) or 4-CF_3-1,2-HOPTO (−250.5). The more negative bonding energy of 4-CH_3-1,2-HOPTO stems from both its more favorable electrostatic (ΔE_{elst} = −259.9 kcal mol^{-1}) and orbital (ΔE_{orb} = −103.3 kcal mol^{-1}) interactions with Tp^CZn. By contrast, the Tp^CZn(4-CF_3-1,2-HOPTO) complex has less stabilization from electrostatic (ΔE_{elst} = −242.6 kcal mol^{-1}) and orbital interaction (ΔE_{orb} = −99.0 kcal mol^{-1}) effects. This trend in bonding energy observed for 1,2-HOPTO derivatives illustrates the respective electron donating and electron withdrawing effects of the methyl and fluoromethyl substituents. Indeed, charge distributions obtained for Tp^CZn(4-CH_3-1,2-HOPTO) and Tp^CZn(4-CF_3-1,2-HOPTO) complexes show the latter to possess less negative charge on its S and O donor atoms (see Supporting Information, Figure S16).

Table 3. Decomposition of Bonding Energies for 1,2-HOPTO Derivatives Bound to the Tp^CZn Scaffold

substituent		–	4-CH_3	4-CF_3
"ideal"[a]	ΔE_{elst}[c]	−257.6	−259.9	−242.6
	ΔE_{orb}[d]	−101.1	−103.3	−99.0
	ΔE_{steric}[e]	95.0	96.4	91.1
	ΔE_{tot}[f]	**−263.7**	**−266.9**	**−250.5**
"protein"[b]	ΔE_{elst}	−242.5	−245.4	−228.2
	ΔE_{orb}	−97.1	−99.1	−95.5
	ΔE_{steric}	84.4	86.1	81.1
	ΔE_{tot}	**−255.2**	**−258.3**	**−242.5**

[a]Results from EDAs performed on "ideal" geometries, corresponding to freely optimized Tp^CZn(MBP) complexes. [b]Results from EDAs performed with the MBP in complex with Tp^CZn constrained to the orientation observed in the crystal structure of 1,2-HOPTO bound to hCAII. [c]The electrostatic interaction energy between Tp^CZn and the MBP. [d]The orbital interaction energy between Tp^CZn and the MBP. This term in the EDA implicitly accounts for charge transfer, polarization, and electron bonding effects.[69,71] [e]The Pauli repulsion energy associated with the bonding of Tp^CZn and the MBP. [f]The total bonding energy between Tp^CZn and the MBP: $\Delta E_{tot} = \Delta E_{elst} + \Delta E_{orb} + \Delta E_{steric}$.[69,71] Further details regarding the EDAs are included in the Supporting Information.

The ordering of 1,2-HOPTO bonding energies is similar when the MBP orientation is constrained to its protein geometry (Table 3, "Protein"), however, the strengths of the individual interactions are significantly diminished when the MBP orientation is distorted. For instance, the values of ΔE_{elst} and ΔE_{orb} in the protein orientation are respectively shifted 15.1 and 4.2 kcal mol^{-1} more positive compared to their values when the MBP geometry is freely optimized. Consequently, the total bonding energies of Tp^CZn(MBP) complexes having MBP orientations constrained to that of their hCAII complexes are approximately 8 kcal mol^{-1} higher in energy (less favorable) than geometries in which the MBP is freely optimized (Table 3).

While the aforementioned bonding energies suggest the hCAII active site Zn^{2+} should preferentially bind, in order, 4-CH_3-1,2-HOPTO, 1,2-HOPTO, and 4-CF_3-1,2-HOPTO, the relative nonpolar binding free energies ($\Delta\Delta G_{np}$, see Supporting Information, Figure S17) obtained from thermodynamic integration (TI) computations for these MBPs in complex with hCAII oppose this energetic ordering. With respect to 4-CF_3-1,2-HOPTO, the values for $\Delta\Delta G_{np}$ of the 4-CH_3-1,2-HOPTO and 1,2-HOPTO MBPs are 0.8 and 1.8 kcal mol^{-1} higher in energy (see Supporting Information, Table S2). These relative energies estimate the nonpolar interactions between the different MBPs and the hydrophobic wall in the

dx.doi.org/10.1021/jm500984b | J. Med. Chem. 2014, 57, 7126−7135

hCAII active site, indicating that the 4-CF_3 substituent forms the strongest interaction. It should be noted that these values are intended to describe the individual forces driving MBP binding and are not meant to be quantitative descriptions of the full binding affinity of the MBPs to hCAII.

DISCUSSION

The results described above demonstrate that relatively minor changes in MBP structure can have a drastic effect on both the affinity and binding mode in a metalloenzyme active site. A wide variety of forces play a part including ligand electrostatics, steric restrictions of the active site, and interactions between the MBP and the active site environment. By examining the binding of 4,6-$(CH_3)_2$-1,2-HOPTO, which maintains bidentate coordination due to stabilization by the methyl group in the 4-position, the origin of monodentate binding by 6-CH_3-1,2-HOPTO in the active site of hCAII could be determined. When the MBP adopts bidentate coordination, the methyl group in the 6-position extends toward the hydrophilic side of the active site, disrupting the highly ordered water network (Figure 7). Two water molecules (W2 and W3) are displaced

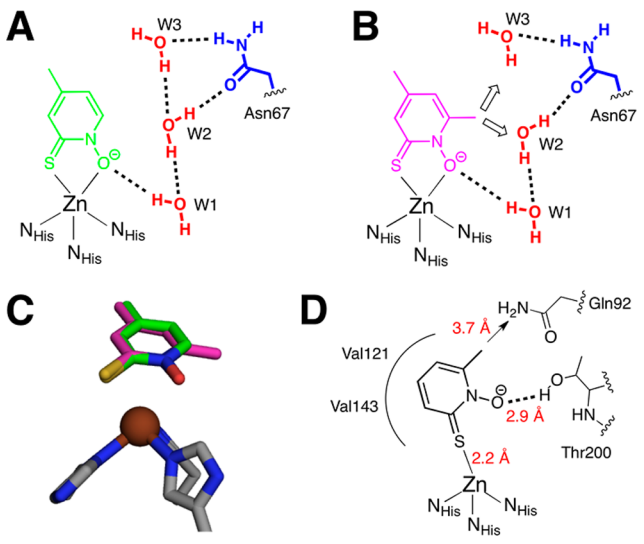

Figure 7. Comparison of the crystal structures of 4-CH_3-1,2-HOPTO (A) and 4,6-$(CH_3)_2$-1,2-HOPTO (B) bound to hCAII reveals disruption of the highly ordered active site water network. (C) The two MBPs essentially overlay, suggesting that the water network disruption is responsible for the ~25-fold decrease in potency for 4,6-$(CH_3)_2$-1,2-HOPTO compared to 4-CH_3-1,2-HOPTO. (D) The monodentate binding mode of 6-CH_3-1,2-HOPTO is stabilized by a hydrogen bond with Thr200 and hydrophobic interactions with Val143, Val121, and Gln92.

by >0.8 Å as a result of the methyl group, breaking a hydrogen bond between them (O−O distances of 4.3 and 2.8 Å in the 4,6-$(CH_3)_2$-1,2-HOPTO and 4-CH_3-1,2-HOPTO structures, respectively). A third water molecule (W1) is displaced by ~0.2 Å, resulting in a longer interaction with the Zn^{2+}-bound oxygen atom (O−O distances of 2.9 and 3.1 Å in the 4-CH_3-1,2-HOPTO and 4,6-$(CH_3)_2$-1,2-HOPTO complexes, respectively). We conclude that in order to avoid these unfavorable interactions, 6-CH_3-1,2-HOPTO adopts monodentate coordination in the active site of hCAII.

Given the favorable interactions formed between the methyl groups of 3-CH_3-1,2-HOPTO and the hydrophobic wall of the active site, it is surprising that 5- and 6-CH_3-1,2-HOPTO do not "flip" in the active site to form similar contacts (Figure 8). This suggests that there is a significant penalty for changing the

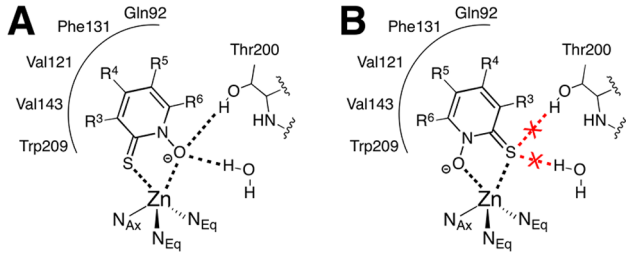

Figure 8. Schematic of the two bidentate conformations available for 1,2-HOPTO. (A) The binding mode observed for unsubstituted 1,2-HOPTO. In addition to binding the metal ion, interactions between the Zn^{2+}-bound oxygen atom and the hydrophilic active site environment are observed. (B) When the ligand is "flipped" 180°, as with 5-CF_3-1,2-HOPTO, the interactions with the hydrophilic environment are weakened and the anionic oxygen atom is positioned near the hydrophobic wall of the active site.

positions of the O and S donor atoms, which likely originates from several features, including (1) Coordination preferences: small-molecule model complexes of His_3Zn active sites coordinated by bidentate (*O*,*S*)-donor ligands exclusively show the sulfur and oxygen atoms as the equatorial and axial donors, respectively.[11,29,30,40−42] Geometry optimizations of Tp^C(1,2-HOPTO) complexes indicate having the *O*-donor coordinate axially is only slightly preferred (ΔE < 0.7 kcal mol^{-1}), thus indicating there is a small penalty for donor-swapping in the absence of a protein environment. (2) Active site electrostatics: If the donors were to swap, the greater anionic charge on the oxygen would be positioned closer to the hydrophobic side of the active site in hCAII, which would be accompanied by an energetic penalty. (3) Hydrogen bonding: The interaction between the active site water/hydrogen bonding network and the Zn^{2+}-bound donor atom would be significantly weakened with a sulfur atom instead of oxygen atom (Figure 8B, shown in red).[43]

Unlike its methyl analogue, 5-CF_3-1,2-HOPTO does, in fact, adopt a "flipped" coordination mode (Figure 8B) in the active site of hCAII. The primary reason for this is likely the greatly improved vdW interaction between the trifluoromethyl group and the hydrophobic wall compared to CH_3. Indeed, the nonpolar contributions of having different hydrophobic groups attached to the 4-position of 1,2-HOPTO are quantified by thermodynamic integration (TI) computations performed on a classical representation of the hCAII(MBP) complexes and indicate that the 4-CF_3 group provides 0.8 kcal mol^{-1} stabilization over the 4-CH_3 group which, in turn, is favored by 1.0 kcal mol^{-1} over unsubstituted 1,2-HOPTO (see Supporting Information, Table S2). Despite a likely weakening of metal coordination in 4-CF_3-1,2-HOPTO compared to 4-CH_3-1,2-HOPTO (due to the electron-withdrawing nature of the trifluoromethyl group), these improved interactions yield excellent activity for the trifluoromethyl derivative. In the case of 3-CF_3-1,2-HOPTO, the vdW contacts are not improved enough to compensate for the loss in metal binding affinity, resulting in lower inhibition compared to its methyl analogue. In addition, the trifluoromethyl derivatives show diminished interactions with Thr200, most likely due to the electron-withdrawing nature of the trifluoromethyl group. The O−O distance for this interaction increases significantly for both CF_3

dx.doi.org/10.1021/jm500984b | J. Med. Chem. 2014, 57, 7126−7135

derivatives relative to their methyl analogues (4.0 Å vs 3.0 and 3.7 Å vs 2.9 Å for 3-CF_3-1,2-HOPTO and 4-CF_3-1,2-HOPTO, respectively), mostly due to a change in the position of the side chain of Thr200 rather than a change in the position of the MBP. The observation of a "flipped" coordination mode for 5-CF_3-1,2-HOPTO is likely a result of both the improved vdW interactions (stabilizing the "flipped" conformation, Figure 8B) as well as decreased anionic character on the Zn^{2+}-bound oxygen atom (destabilizing the "normal" conformation, Figure 8A).

MPy-4CH_3, which binds in the same conformation as 4-CH_3-1,2-HOPTO, but makes no interactions through the endocyclic nitrogen, is 250-fold less potent. This suggests that the interactions between the anionic oxygen and both the Zn^{2+} ion and the hydrophilic active site environment make a significant contribution to the affinity of 1,2-HOPTO. However, it is important to note that the pK_a of MPy-4CH_3 is significantly higher than that of 1,2-HOPTO and it is therefore likely to bind as a neutral species. In this respect, the low binding affinity of MPy-4CH_3 also underscores the importance of ligand electrostatics. Molecules with sulfur as an anionic donor atom (thiophenols) are very potent, while analogous compounds with less anionic character on the sulfur (1,2-HOPTO derivatives) show lower affinity; those with little to no anionic character on the sulfur (2-mercaptopyridines) show an even greater decrease in binding. While this result would seem to indicate that the sulfur donor plays a limited role in the binding of 1,2-HOPTO derivatives to hCAII, exclusion of a second donor atom entirely (PyNO-4CH_3) results in a molecule with no observable activity, and replacing the sulfur with oxygen (4-CH_3-1,2-HOPO) results in a greater than 30-fold decrease in binding affinity. Further demonstrating the intricacies of metal coordination in the hCAII active site, aliphatic thiols such as 2-mercaptoethanol have been shown to lack inhibitory activity, underscoring the importance of the aromatic ring system.[44]

The diminished inhibition for 1,2-HOPO relative to that of the 1,2-HOPTO also supports the case for considering these molecular scaffolds as pharmacophores and not chelators. The Zn^{2+} affinity in free solution is comparable for 1,2-HOPO and 1,2-HOPTO (K_d of 5−10 μM, Figure 9),[45] but their affinities to Zn^{2+} ion active sites in metalloproteins is highly variable. In the case of anthrax lethal factor, both MBPs show weak affinity (IC_{50} ~5 mM),[46] while with matrix metalloproteinases[11] and hCAII, the 1,2-HOPTO MBP is significantly more potent (~50-fold) than 1,2-HOPO.

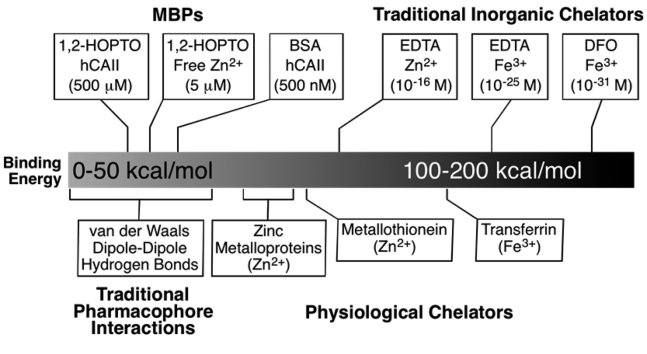

Figure 9. Binding affinities of MBPs such as 1,2-HOPTO and benzenesulfonamide (BSA) are much closer to traditional pharmacophores than to conventional metal chelators. Examples of such chelators include ethylenediaminetetraacetic acid (EDTA) and deferoxamine (DFO). The affinity of MBPs for metal ions are also well below those of metalloproteins (e.g., zinc fingers, hCAII, etc.) and regulatory proteins such as metallothioneins and transferrin, indicative of the pharamcophore nature of these functional groups.

CONCLUSION

Both the coordination mode and affinity of metal-binding pharmacophores (MBPs) can be significantly influenced by other interactions within the active site environment. Depending on its position, a peripheral methyl substituent on the 1,2-HOPTO scaffold can cause either a greater than 10-fold increase in potency against hCAII (4-CH_3-1,2-HOPTO) or a 5-fold decrease in potency accompanied by a shift to monodentate coordination to the active site Zn^{2+} ion (6-CH_3-1,2-HOPTO). Despite greatly improved interactions with the surrounding active site, 4-CF_3-1,2-HOPTO only shows a slight increase in potency relative to its methyl analogue due to a weakening of MBP-metal binding. While the inhibitory activity of a MBP is unquestionably influenced by the strength of metal coordination, our findings indicate that the interactions formed between the MBP and the surrounding active site environment upon binding are equally important. Furthermore, the affinities of MBPs for active site metal ions are much closer to those observed for traditional pharmacophore−protein interactions than to those of known metal chelators (Figure 9).[47−51] It is thus more appropriate to consider the metal-binding portion of metalloprotein inhibitors as pharmacophores rather than chelators. By recognizing the pharmacophore nature of these functional groups, we can use appropriate design principles to optimize MBPs, not only for metal coordination but also for other interactions with the target active site, in a rational and effective manner.

METHODS

Synthesis. MBPs were synthesized using a modified version of previously reported procedures.[52,53] Details can be found in the Supporting Information.

hCAII Activity Assay. hCAII was expressed and purified as previously reported,[54] and a detailed procedure can be found in the Supporting Information. Assays were performed in 50 mM HEPES, pH 8.0, containing Na_2SO_4 to an ionic strength of 100 mM. Enzyme (100 nM final concentration) was incubated with varying concentrations of inhibitor for 10 min at room temperature before the addition of substrate (*p*-nitrophenyl acetate, final concentration between 0.05 and 10 mM). The reaction was monitored by the increase in absorbance at 405 nm. Initial reaction rates vs substrate concentration were plotted for three concentrations of inhibitor and the curves simultaneously fit for K_i using GraphPad Prism. Representative examples of curve fitting can be found in the Supporting Information (Figure S1).

hCAII Crystallization. Crystals of hCAII were obtained by the sitting-drop or hanging-drop vapor diffusion method. The protein solution consisted of 20 mg/mL hCAII and 1 mM *p*-chloromercuribenzoic acid in 50 mM Tris-SO_4, pH 8.0. The precipitant solution contained 2.7−3.0 M $(NH_4)_2SO_4$ in 50 mM Tris-SO_4 pH 8.15. Drops consisted of 3 μL of protein solution plus 2.5−4.0 μL of precipitant solution and were equilibrated at 18 °C against 750 μL of precipitant solution. Crystals roughly 0.3 × 0.3 × 0.3 mm in size appeared after 2 days to 3 weeks depending on the drop size and precipitant concentration. Once formed, crystals were transferred to 15 μL of soak solutions containing MBP (at saturation, generally ~1 mM), 1.5 M sodium citrate, 50 mM HEPES, pH 8.15, 5% glycerol, and 1−5% DMSO. Soak solutions of 3-CH_3-TP and 4-CH_3-2MP also contained 2 mM tris(carboxyethyl)phosphine (TCEP) as a reducing agent. Crystals were taken directly from the soak solutions for data collection.

dx.doi.org/10.1021/jm500984b | J. Med. Chem. 2014, 57, 7126−7135

Crystal Structure Determination. X-ray diffraction studies on hCAII crystals were carried out at 100 K with a Bruker D8 Smart 6000 CCD detector and utilizing Cu Kα radiation (λ = 1.5478 Å) from a Bruker-Nonius FR-591 rotating anode generator. The data were integrated and scaled using the Bruker APEX software suite. All crystals belonged to the monoclinic space group $P2_1$. The data were phased by molecular replacement using a previously reported hCAII structure (PDB 3KS3[55]) with water molecules removed. Models were built by alternating refinement using REFMAC5[56] and manual visualization and model building in Coot.[57] Ligand topologies were generated using the PRODRG server.[58] The structures contain *p*-mercuribenzoic acid bound to Cys206. Complete data collection and refinement statistics can be found in the Supporting Information (Table S1).

Density Functional Computations. To assess MBP binding modes in the absence of a protein environment, geometry optimizations were performed utilizing a tris(5-methylpyrazolyl)-methane scaffold, referred to here as $Tp^{C}Zn$ (see Supporting Information, Figure S3). This is a modification of the $Tp^{Ph,Me}Zn$ ($Tp^{Ph,Me}$ = hydrotris(5,3-methylphenylpyrazolyl)borate) model complex commonly used experimentally to study MBP coordination.[11,26−30] In addition to omitting the phenyl groups of the $Tp^{Ph,Me}$ ligand to eliminate steric bulk, the $Tp^{C}Zn$ system provides a rigid scaffold with the correct net charge (q = +2) for modeling the hCAII His_3Zn center in a computationally efficient manner.

Geometry optimizations are performed with Gaussian 09,[59] using Becke's three-parameter hybrid method with the Lee, Yang, and Parr correlation functional (B3LYP)[60−63] and the 6-311++G(2d,2p) basis set. This level of theory has previously been used to successfully recapitulate geometric parameters of model active sites for Zn^{2+} metalloproteins[64] as well as free energies of water−chloride exchange in zinc chloride complexes.[65] Further, implicit solvation is employed in all computations using the conductor-like polarizable continuum model (CPCM) with ε = 10,[66−68] consistent with the crystallization environment previously used to structurally characterize $Tp^{Ph,Me}Zn$-(MBP) complexes.[35] Where indicated, energy decomposition analyses[69−71] were performed on the optimized geometries of $Tp^{C}Zn$(MBP) complexes using the Amsterdam Density Functional 2009 suite of programs[71,72] to enable assessments of electrostatic, steric (Pauli repulsion), and orbital (which accounts for charge transfer, polarization, and electron pair bonding effects) contributions to the bond energy between $Tp^{C}Zn$ and the different MBPs. Additional details and explanations can be found in the Supporting Information.

Thermodynamic Integration Computations. The difference in the nonpolar free energies of two MBPs (denoted by MBP_A and MBP_B) binding to hCAII ($\Delta\Delta G_{np}$) is estimated from eq 1:

$$\Delta\Delta G_{np} = \Delta G_{np}^{A\rightarrow B(bound)} - \Delta G_{np}^{A\rightarrow B(unbound)} \quad (1)$$

In eq 1, $\Delta G_{np}{}^{A\rightarrow B(bound)}$ and $\Delta G_{np}{}^{A\rightarrow B(unbound)}$ correspond to the "alchemical transformations" of MBP_A to MBP_B when, respectively, bound to hCAII and free in solution. The value of $\Delta G_{np}{}^{A\rightarrow B(bound)}$ is obtained using thermodynamic integration (TI):[73−75]

$$\Delta G_{np}^{A\rightarrow B(bound)} \approx \int_{\lambda=0}^{\lambda=1} \left\langle \frac{\partial V(\lambda)}{\partial \lambda} \right\rangle d\lambda \quad (2)$$

where $V(\lambda)$ is the potential energy as a function of λ, a coupling parameter that varies the potential from being defined by the hCAII(MBP_A) complex (λ = 0) to being defined by the hCAII:MBP_B complex (λ = 1). The brackets in eq 2 indicate ensemble averaging at a given value of λ, and integration is performed numerically using the trapezoidal rule. An analogous procedure is used to compute $\Delta G_{np}{}^{A\rightarrow B(unbound)}$.

All TI computations are performed using the pmemd molecular dynamics (MD) engine[76] in the AMBER14 suite of programs.[77] Simulation details and analyses of TI results are reported in the Supporting Information.

■ ASSOCIATED CONTENT

Ⓢ Supporting Information

Full experimental details for ligand synthesis, protein expression and purification, crystal structure collection details and refinement statistics, and complete computational procedures. This material is available free of charge via the Internet at http://pubs.acs.org.

Accession Codes

Coordinate and structure factor files for all hCAII structures have been deposited with the Protein Data Bank: 4Q7P, 4Q7S, 4Q7V, 4Q7W, 4Q81, 4Q83, 4Q87, 4Q8X, 4Q8Y, 4Q8Z, 4Q90, 4Q9Y, 4Q99.

■ AUTHOR INFORMATION

Corresponding Author

*Phone: 858-822-5596. Fax: 858-822-5598. E-mail: scohen@ucsd.edu.

Notes

The authors declare no competing financial interest.

■ ACKNOWLEDGMENTS

J.A.M. acknowledges support from the National Institutes of Health (NIH GM31749), National Science Foundation (MCB-1020765), Howard Hughes Medical Institute, National Biomedical Computation Resource, and NSF supercomputer centers. P.G.B. acknowledges support from the National Institutes of Health Molecular Biophysics Training Grant (2T32GM008326-21). S.M.C. acknowledges support from the National Institutes of Health (R01 GM098435). D.P.M. is supported by a SMART scholarship from the Office of the Secretary of Defense−Test and Evaluation (N00244-09-1-0081).

■ REFERENCES

(1) Anzellotti, A. I.; Farrell, N. P. Zinc Metalloproteins as Medicinal Targets. *Chem. Soc. Rev.* **2008**, *37*, 1629−1651.

(2) Rouffet, M.; Cohen, S. M. Emerging Trends in Metalloprotein Inhibition. *Dalton Trans.* **2011**, *40*, 3445−3454.

(3) Supuran, C. T.; Scozzafava, A.; Casini, A. Carbonic Anhydrase Inhibitors. *Med. Res. Rev.* **2003**, *23* (2), 146−189.

(4) Brown, N. J.; Vaughan, D. E. Angiotensin-Converting Enzyme Inhibitors. *Circulation* **1998**, *97*, 1411−1420.

(5) Paris, M.; Porcelloni, M.; Binaschi, M.; Fattori, D. Histone Deacetylase Inhibitors: From Bench to Clinic. *J. Med. Chem.* **2008**, *51* (6), 1505−1529.

(6) Young, R. N. Inhibitors of 5-Lipoxygenase: A Therapeutic Potential Yet to be Fully Realized? *Eur. J. Med. Chem.* **1999**, *34*, 671−685.

(7) Fernández-Montero, J. V.; Vispo, E.; Soriano, V. Emerging Antiretroviral Drugs. *Expert Opin. Pharmacother.* **2014**, *15* (2), 211−219.

(8) Martin, D. P.; Puerta, D. T.; Cohen, S. M., Metalloprotein Inhibitors. In *Ligand Design in Medicinal Inorganic Chemistry*; Storr, T., Ed.; John Wiley and Sons, Inc.: Hoboken, NJ, 2014.

(9) Moradei, O.; Vaisburg, A.; Martell, R. E. Histone Deacetylase Inhibitors in Cancer Therapy: New Compounds and Clinical Update of Benzamide-Type Agents. *Curr. Top. Med. Chem.* **2008**, *8* (10), 841−858.

(10) Jacobsen, J. A.; Fullagar, J. L.; Miller, M. T.; Cohen, S. M. Identifying Chelators for Metalloprotein Inhibitors Using a Fragment-Based Approach. *J. Med. Chem.* **2011**, *54* (2), 591−602.

(11) Puerta, D. T.; Lewis, J. A.; Cohen, S. M. New Beginnings for Matrix Metalloproteinase Inhibitors: Identification of High-Affinity Zinc-Binding Groups. *J. Am. Chem. Soc.* **2004**, *126* (27), 8388−8389.

(12) Puerta, D. T.; Mongan, J.; Tran, B. L.; McCammon, J. A.; Cohen, S. M. Potent, Selective Pyrone-Based Inhibitors of Stromelysin-1. *J. Am. Chem. Soc.* **2005**, *127*, 14148−14149.
(13) Agrawal, A.; Romero-Perez, D.; Jacobsen, J. A.; Villarreal, F. J.; Cohen, S. M. Zinc-Binding Groups Modulate Selective Inhibition of MMPs. *ChemMedChem* **2008**, *3* (5), 812−820.
(14) Rouffet, M.; de Oliveira, C. A. F.; Udi, Y.; Agrawal, A.; Sagi, I.; McCammon, J. A.; Cohen, S. M. From Sensors to Silencers: Quinoline- and Benzimidazole-Sulfonamides as Inhibitors for Zinc Proteases. *J. Am. Chem. Soc.* **2010**, *132* (24), 8232−8233.
(15) Agrawal, A.; DeSoto, J.; Fullagar, J. L.; Maddali, K.; Rostami, S.; Richman, D. D.; Pommier, Y.; Cohen, S. M. Probing Chelation Motifs in HIV Integrase Inhibitors. *Proc. Natl. Acad. Sci. U. S. A.* **2012**, *109* (7), 2251−2256.
(16) Garner, A. L.; Struss, A. K.; Fullagar, J. L.; Agrawal, A.; Moreno, A. Y.; Cohen, S. M.; Janda, K. D. 3-Hydroxy-1-alkyl-2-methylpyridine-4(1*H*)-thiones: Inhibition of the *Pseudomonas aeruginosa* Virulence Factor LasB. *ACS Med. Chem. Lett.* **2012**, *3* (8), 668−672.
(17) Rogolino, D.; Carcelli, M.; Sechi, M.; Neamati, N. Viral enzymes containing magnesium: Metal binding as a successful strategy in drug design. *Coord. Chem. Rev.* **2012**, *256* (23−24), 3063−3086.
(18) Flagg, S. C.; Martin, C. B.; Taabazuing, C. Y.; Holmes, B. E.; Knapp, M. J. Screening Chelating Inhibitors of HIF-Prolyl Hydroxylase Domain 2 (PHD2) and Factor Inhibiting HIF (FIH). *J. Inorg. Biochem.* **2012**, *113*, 25−30.
(19) Johnson, S.; Barile, E.; Farina, B.; Purves, A.; Wei, J.; Chen, L.-H.; Shiryaev, S.; Zhang, Z.; Rodionova, I.; Agrawal, A.; Cohen, S. M.; Osterman, A.; Strongin, A.; Pellecchia, M. Targeting Metalloproteins by Fragment-Based Lead Discovery. *Chem. Biol. Drug Des.* **2011**, *78*, 211−223.
(20) Madsen, A. S.; Kristensen, H. M. E.; Lanz, G.; Olsen, C. A. The Effect of Various Zinc Binding Groups on Inhibition of Histone Deacetylases. *ChemMedChem* **2014**, *9* (3), 614−626.
(21) Deng, L.; Sundriyal, S.; Rubio, V.; Shi, Z.-z.; Song, Y. Coordination Chemistry Based Approach to Lipophilic Inhibitors of 1-Deoxy-D-xylulose-5-phosphate Reductoisomerase. *J. Med. Chem.* **2009**, *52* (21), 6539−6542.
(22) Patil, V.; Sodji, Q. H.; Kornacki, J. R.; Mrksich, M.; Oyelere, A. K. 3-Hydroxypridin-2-thione as Novel Zinc Binding Group for Selective Histone Deacetylase Inhibition. *J. Med. Chem.* **2013**, *56* (9), 3492−3506.
(23) Pottel, J.; Therrien, E.; Gleason, J. L.; Moitessier, N. Docking Ligands into Flexible and Solvated Macromolecules. 6. Development and Application to the Docking of HDACs and other Zinc Metalloenzyme Inhibitors. *J. Chem. Inf. Model.* **2014**, *54*, 254−265.
(24) Zhang, J.; Yang, W.; Piquemal, J.-P.; Ren, P. Modeling Structural Coordination and Ligand Binding in Zinc Proteins with a Polarizable Potential. *J. Chem. Theory Comput.* **2012**, *8*, 1314−1324.
(25) Seebeck, B.; Reulecke, I.; Kämper, A.; Rarey, M. Modeling of Metal Interaction Geometries for Protein−Ligand Docking. *Proteins* **2008**, *71*, 1237−1254.
(26) Looney, A.; Han, R.; McNeill, K.; Parkin, G. Tris(pyrazoly1)-hydroboratozinc Hydroxide Complexes as Functional Models for Carbonic Anhydrase: On the Nature of the Bicarbonate Intermediate. *J. Am. Chem. Soc.* **1993**, *115*, 4690−4697.
(27) Looney, A.; Parkin, G.; Alsfasser, R.; Ruf, M.; Vahrenkamp, H. Zinc Pyrazolylborate Complexes Relevant to the Biological Function of Carbonic Anhydrase. *Angew. Chem., Int. Ed.* **1992**, *31* (1), 92−93.
(28) Parkin, G. Synthetic Analogues Relevant to the Structure and Function of Zinc Enzymes. *Chem. Rev.* **2004**, *104* (2), 699−767.
(29) Puerta, D. T.; Cohen, S. M. Elucidating Drug−Metalloprotein Interactions with Tris(pyrazolyl)borate Model Complexes. *Inorg. Chem.* **2002**, *41* (20), 5075−5082.
(30) Puerta, D. T.; Schames, J. R.; Henchman, R. H.; McCammon, J. A.; Cohen, S. M. From Model Complexes to Metalloprotein Inhibition: A Synergistic Approach to Structure-Based Drug Discovery. *Angew. Chem., Int. Ed.* **2003**, *42* (32), 3772−3774.
(31) Cho, J. H.; Kim, D. H.; Chung, S. J.; Ha, N.-C.; Oh, B.-H.; Choi, K. Y. Insight into the Stereochemistry in the Inhibition of Carboxypeptidase A with *N*-(hydroxyaminocarbonyl)phenylalanine: Binding Modes of an Enantiomeric Pair of the Inhibitor to Carboxypeptidase A. *Bioorg. Med. Chem.* **2002**, *10*, 2015−2022.
(32) Gaucher, J. F.; Selkti, M.; Tiraboschi, G.; Prangé, T.; Roques, B. P.; Tomas, A.; Fournié-Zaluski, M. C. Crystal Structures of α-Mercaptoacyldipeptides in the Thermolysin Active Site: Structural Parameters for a Zn Monodentation or Bidentation in Metalloendopeptidases. *Biochemistry* **1999**, *38* (39), 12569−12576.
(33) Bauman, J. D.; Patel, D.; Baker, S. F.; Vijayan, R. S. K.; Xiang, A.; Parhi, A. K.; Martínez-Sobrido, L.; LaVoie, E. J.; Das, K.; Arnold, E. Crystallographic Fragment Screening and Structure-Based Optimization Yields a New Class of Influenza Endonuclease Inhibitors. *ACS Chem. Biol.* **2013**, *8*, 2501−2508.
(34) Krishnamurthy, V. M.; Kaufman, G. K.; Urbach, A. R.; Gitlin, I.; Gudiksen, K. L.; Weibel, D. B.; Whitesides, G. M. Carbonic Anhydrase as a Model for Biophysical and Physical−Organic Studies of Proteins and Protein−Ligand Binding. *Chem. Rev.* **2008**, *108* (3), 946−1051.
(35) Martin, D. P.; Blachly, P. G.; Marts, A. R.; Woodruff, T. M.; Oliveira, C. A. F. d.; McCammon, J. A.; Tierney, D. L.; Cohen, S. M. 'Unconventional' Coordination Chemistry by Metal Chelating Fragments in a Metalloprotein Active Site. *J. Am. Chem. Soc.* **2014**, *136* (14), 5400−5406.
(36) Wischeler, J. S.; Innocenti, A.; Vullo, D.; Agrawal, A.; Cohen, S. M.; Heine, A.; Supuran, C. T.; Klebe, G. Bidentate Zinc Chelators for α-Carbonic Anhydrases that Produce a Trigonal Bipyramidal Coordination Geometry. *ChemMedChem* **2010**, *5* (9), 1609−1615.
(37) Kawai, K.; Nagata, N. Metal−Ligand Interactions: An Analysis of Zinc Binding Groups Using the Protein Data Bank. *Eur. J. Med. Chem.* **2012**, *51*, 271−276.
(38) Barrese, A. A.; Genis, C.; Fisher, S. Z.; Orwenyo, J. N.; Kumara, M. T.; Dutta, S. K.; Phillips, E.; Kiddle, J. J.; Tu, C.; Silverman, D. N.; Govindasamy, L.; Agbandje-McKenna, M.; McKenna, R.; Tripp, B. C. Inhibition of Carbonic Anhydrase II by Thioxolone: A Mechanistic and Structural Study. *Biochemistry* **2008**, *47* (10), 3174−3184.
(39) Martin, D. P.; Hann, Z. S.; Cohen, S. M. Metalloprotein−Inhibitor Binding: Human Carbonic Anhydrase II as a Model for Probing Metal−Ligand Interactions in a Metalloprotein Active Site. *Inorg. Chem.* **2013**, *52* (21), 12207−12215.
(40) Brayton, D.; Jacobsen, F. E.; Cohen, S. M.; Farmer, P. J. A Novel Heterocyclic Atom Exchange Reaction with Lawesson's Reagent: A One-Pot Synthesis of Dithiomaltol. *Chem. Commun.* **2006**, 206−208.
(41) Tekeste, T.; Vahrenkamp, H. Modeling Zinc Enzyme Inhibition with Functional Thiolate Ligands. *Inorg. Chem.* **2006**, *45* (26), 10799−10806.
(42) Puerta, D. T.; Cohen, S. M. Examination of Novel Zinc-Binding Groups for Use in Matrix Metalloproteinase Inhibitors. *Inorg. Chem.* **2003**, *42* (11), 3423−3430.
(43) Platts, J. A.; Howard, S. T.; Bracke, B. R. F. Directionality of Hydrogen Bonds to Sulfur and Oxygen. *J. Am. Chem. Soc.* **1996**, *118* (11), 2726−2733.
(44) Innocenti, A.; Hilvo, M.; Scozzafava, A.; Lindfors, M.; Nordlund, H. R.; Kulomaa, M. S.; Parkkila, S.; Supuran, C. T. Carbonic Anhydrase Inhibitors: The Very Weak Inhibitors Dithiothreitol, B-Mercaptoethanol, Tris(carboxyethyl)phosphine and Threitol Interfere with the Binding of Sulfonamides to Isozymes II and IX. *Bioorg. Med. Chem. Lett.* **2008**, *18* (6), 1898−1903.
(45) Sun, P.-J.; Fernando, Q.; Freiser, H. Formation Constants of Transition Metal Complexes of 2-Hydroxypyridine-1-oxide and 2-Mercaptopyridine-1-oxide. *Anal. Chem.* **1964**, *36* (13), 2485−2488.
(46) Lewis, J. A.; Mongan, J.; McCammon, J. A.; Cohen, S. M. Evaluation and Binding Mode Prediction of Thiopyrone-Based Inhibitors of Anthrax Lethal Factor. *ChemMedChem* **2006**, *1* (7), 694−697.
(47) Aisen, P.; Leibman, A.; Zweier, J. Stoichiometric and Site Characteristics of the Binding of Iron to Human Transferrin. *J. Biol. Chem.* **1978**, *253* (6), 1930−1937.
(48) Smith, R. M.; Martell, A. E. Critical Stability Constants, Enthalpies and Entropies for the Formation of Metal Complexes of

Aminopolycarboxylic Acids and Carboxylic Acids. *Sci. Total Environ.* **1987**, *64*, 125−147.
(49) Palmiter, R. D. Protection Against Zinc Toxicity by Metallothionein and Zinc Transporter 1. *Proc. Natl. Acad. Sci. U. S. A.* **2004**, *101* (14), 4918−4923.
(50) Reddi, A. R.; Guzman, T. R.; Breece, R. M.; Tierney, D. L.; Gibney, B. R. Deducing the Energetic Cost of Protein Folding in Zinc Finger Proteins Using Designed Metallopeptides. *J. Am. Chem. Soc.* **2007**, *129* (42), 12815−12827.
(51) Yu, Y.; Gutierrez, E.; Kovacevic, Z.; Saletta, F.; Obeidy, P.; Rahmanto, Y. S.; Richardson, D. R. Iron Chelators for the Treatment of Cancer. *Curr. Med. Chem.* **2012**, *19* (17), 2689−2702.
(52) Agrawal, A.; de Oliveira, C. A. F.; Cheng, Y.; Jacobsen, J. A.; McCammon, J. A.; Cohen, S. M. Thioamide Hydroxypyrothiones Supersede Amide Hydroxypyrothiones in Potency against Anthrax Lethal Factor. *J. Med. Chem.* **2009**, *52* (4), 1063−1074.
(53) Abramovitch, R. A.; Knaus, E. E. The Direct Thionation and Aminoalkylation of Pyridine 1-oxides and Related Reactions. *J. Heterocycl. Chem.* **1975**, *12* (4), 683−690.
(54) Martin, D. P.; Cohen, S. M. Nucleophile Recognition as an Alternative Inhibition Mode for Benzoic Acid Based Carbonic Anhydrase Inhibitors. *Chem. Commun.* **2012**, *48*, 5259−5261.
(55) Avvaru, B. S.; Kim, C. U.; Sippel, K. H.; Gruner, S. M.; Agbandje-McKenna, M.; Silverman, D. N.; McKenna, R. A Short, Strong Hydrogen Bond in the Active Site of Human Carbonic Anhydrase II. *Biochemistry* **2010**, *49* (2), 249−251.
(56) Murshudov, G. N.; Vagin, A. A.; Dodson, E. J. Refinement of Macromolecular Structures by the Maximum-Likelihood Method. *Acta Crystallogr., Sect. D.: Biol. Crystallogr.* **1997**, *D53*, 240−255.
(57) Emsley, P.; Cowtan, K. Coot: Model-Building Tools for Molecular Graphics. *Acta Crystallogr., Sect. D: Biol. Crystallogr.* **2004**, *D60*, 2126−2132.
(58) Schüttelkopf, A. W.; Aalten, D. M. F. v. PRODRG: A Tool for High-Throughput Crystallography of Protein−Ligand Complexes. *Acta Crystallogr., Sect. D: Biol. Crystallogr.* **2004**, *D60*, 1355−1363.
(59) Frisch, M. J.; Trucks, G. W.; Schlegel, H. B.; Scuseria, G. E.; Robb, M. A.; Cheeseman, J. R.; Scalmani, G.; Barone, V.; Mennucci, B.; Petersson, G. A.; Nakatsuji, H.; Caricato, M.; Li, X.; Hratchian, H. P.; Izmaylov, A. F.; Bloino, J.; Zheng, G.; Sonnenberg, J. L.; Hada, M.; Ehara, M.; Toyota, K.; Fukuda, R.; Hasegawa, J.; Ishida, M.; Nakajima, T.; Honda, Y.; Kitao, O.; Nakai, H.; Vreven, T.; Montgomery, Jr., J. A.; Peralta, J. E.; Ogliaro, F.; Bearpark, M.; Heyd, J. J.; Brothers, E.; Kudin, K. N.; Staroverov, V. N.; Kobayashi, R.; Normand, J.; Raghavachari, K.; Rendell, A.; Burant, J. C.; Iyengar, S. S.; Tomasi, J.; Cossi, M.; Rega, N.; Millam, J. M.; Klene, M.; Knox, J. E.; Cross, J. B.; Bakken, V.; Adamo, C.; Jaramillo, J.; Gomperts, R.; Stratmann, R. E.; Yazyev, O.; Austin, A. J.; Cammi, R.; Pomelli, C.; Ochterski, J. W.; Martin, R. L.; Morokuma, K.; Zakrzewski, V. G.; Voth, G. A.; Salvador, P.; Dannenberg, J. J.; Dapprich, S.; Daniels, A. D.; Farkas, Ö.; Foresman, J. B.; Ortiz, J. V.; Cioslowski, J.; Fox, D. J. *Gaussian 09*, revision A.1; Gaussian, Inc.: Wallingford, CT, 2009.
(60) Becke, A. D. Density-Functional Thermochemistry 0.3. The Role of Exact Exchange. *J. Chem. Phys.* **1993**, *98* (7), 5648−5652.
(61) Lee, C. T.; Yang, W. T.; Parr, R. G. Development of the Colle−Salvetti Correlation-Energy Formula into a Functional of the Electron Density. *Phys. Rev. B* **1988**, *37* (2), 785−789.
(62) Stephens, P. J.; Devlin, F. J.; Chabalowski, C. F.; Frisch, M. J. Ab Initio Calculation of Vibrational Absorption and Circular-Dichroism Spectra Using Density-Functional Force Fields. *J. Phys. Chem.* **1994**, *98* (45), 11623−11627.
(63) Vosko, S. H.; Wilk, L.; Nusair, M. Accurate Spin-Dependent Electron Liquid Correlation Energies for Local Spin-Density Calculations—A Critical Analysis. *Can. J. Phys.* **1980**, *58* (8), 1200−1211.
(64) Ryde, U. Carboxylate Binding Modes in Zinc Proteins: A Theoretical Study. *Biophys. J.* **1999**, *77* (5), 2777−2787.
(65) Dudev, T.; Lim, C. Tetrahedral vs Octahedral ZincComplexes with Ligands of Biological Interest: A DFT/CDM Study. *J. Am. Chem. Soc.* **2000**, *122* (45), 11146−11153.
(66) Barone, V.; Cossi, M. Quantum Calculation of Molecular Energies and Energy Gradients in Solution by a Conductor Solvent Model. *J. Phys. Chem. A* **1998**, *102* (11), 1995−2001.
(67) Cossi, M.; Rega, N.; Scalmani, G.; Barone, V. Energies, Structures, and Electronic Properties of Molecules in Solution with the C-PCM Solvation Model. *J. Comput. Chem.* **2003**, *24* (6), 669−681.
(68) Klamt, A.; Schuurmann, G. Cosmo—A New Approach to Dielectric Screening in Solvents with Explicit Expressions for the Screening Energy and Its Gradient. *J. Chem. Soc., Perkin Trans. 2* **1993**, No. 5, 799−805.
(69) Bickelhaupt, F. M.; Baerends, E. J. Kohn−Sham density functional theory: predicting and understanding chemistry *Reviews in Computational Chemistry*, Wiley: New York, **2000**; Vol. *15*, pp 1−86.
(70) Kitaura, K.; Morokuma, K. A New Energy Decomposition Scheme for Molecular Interactions Within the Hartree−Fock Approximation. *Int. J. Quantum Chem.* **1976**, *10* (2), 325−340.
(71) te Velde, G.; Bickelhaupt, F. M.; Baerends, E. J.; Guerra, C. F.; Van Gisbergen, S. J. A.; Snijders, J. G.; Ziegler, T. Chemistry with ADF. *J. Comput. Chem.* **2001**, *22* (9), 931−967.
(72) *ADF 2009*; Scientific Computing and Modelling NV, Vrije Universiteit, Theoretical Chemistry: Amsterdam, 2009.
(73) Kollman, P. Free Energy Calculations: Applications to Chemical and Biochemical Phenomena. *Chem. Rev.* **1993**, *93* (7), 2395−2417.
(74) Straatsma, T. P.; McCammon, J. A. Multiconfiguration Thermodynamic Integration. *J. Chem. Phys.* **1991**, *95* (2), 1175.
(75) Straatsma, T. P.; McCammon, J. A. Computational Alchemy. *Annu. Rev. Phys. Chem.* **1992**, *43* (1), 407−435.
(76) Kaus, J. W.; Pierce, L. T.; Walker, R. C.; McCammon, J. A. Improving the Efficiency of Free Energy Calculations in the Amber Molecular Dynamics Package. *J. Chem. Theory Comput.* **2013**, *9* (9), 4131−4139.
(77) Case, D. A.; Darden, T. A.; Cheatham, T. E., III; Simmerling, C. L.; Wang, J; Duke, R. E.; Luo, R.; Walker, R. C.; Zhang, W.; Merz, K. M.; Roberts, B.; Hayik, S.; Roitberg, A.; Seabra, G.; Swails, J.; Götz, A. W.; Kolossváry, I.; Wong, K. F.; Paesani, F.; Vanicek, J.; Wolf, R. M.; Liu, J.; Wu, X.; Brozell, S. R.; Steinbrecher, T.; Gohlke, H.; Cai, Q.; Ye, X.; Wang, J.; Hsieh, M.-J.; Cui, G.; Roe, D. R.; Mathews, D. H.; Seetin, M. G.; Salomon-Ferrer, R.; Sagui, C.; Babin, V.; Luchko, T.; Gusarov, S.; Kovalenko, A.; Kollman, P. A. *AMBER 14*; University of California: San Francisco, 2012.